Author Manuscript

Author Manuscript

Author Manuscript

Author Manuscript

HHS Public Access

Author manuscript

Curr Eye Res. Author manuscript; available in PMC 2017 March 16.

Published in final edited form as:

Curr Eye Res. 2011 October ; 36(10): 947–957. doi:10.3109/02713683.2011.587934.

Single Cell Imaging of the Chick Retina with Adaptive Optics

Kenneth Headington, **Stacey S. Choi**, **Debora Nickla**, and **Nathan Doble**

New England College of Optometry, 424 Beacon Street, Boston, MA 02115

Abstract

Purpose—The chick eye is extensively used as a model in the study of myopia and its progression; however, analysis of the photoreceptor mosaic has required the use of excised retina due to the uncorrected optical aberrations in the lens and cornea. This study implemented high resolution adaptive optics (AO) retinal imaging to visualize the chick cone mosaic *in vivo*.

Methods—The New England College of Optometry (NECO) AO fundus camera was modified to allow high resolution in vivo imaging on 2 six-week-old White Leghorn chicks (*Gallus gallus domesticus*) – labeled chick A and chick B. Multiple, adjacent images, each with a 2.5° field of view, were taken and subsequently montaged together. This process was repeated at varying retinal locations measured from the tip of the pecten. Automated software was used to determine the cone spacing and density at each location. Voronoi analysis was applied to determine the packing arrangement of the cones.

Results—In both chicks, cone photoreceptors were clearly visible at all retinal locations imaged. Cone densities measured at 36° nasal-12° superior retina from the pecten tip for chick A and 40° nasal-12° superior retina for chick B were 21,714±543 and 26,105±653 cones/mm^2 respectively. For chick B, a further 11 locations immediately surrounding the pecten were imaged, with cone densities ranging from 20,980±524 to 25,148±629 cones/mm^2.

Conclusion—*In vivo* analysis of the cone density and its packing characteristics are now possible in the chick eye through AO imaging, which has important implications for future studies of myopia and ocular disease research.

Keywords

adaptive optics; cone; photoreceptors; retinal imaging; chick

1. Introduction

The chick eye is a widely used model in the study of the visual control of ocular growth, due mainly to its robust response to retinal defocus and the rapidity with which these responses are effected.[1] Form deprivation using translucent diffusers that eliminate form vision results in axial elongation and myopic refractive errors within days.[2] Spectacle lens wear causes bi-directional compensation to myopic and hyperopic defocus, resulting in hyperopia and

Correspondence: Dr. Nathan Doble, New England College of Optometry, 424 Beacon Street, Boston, MA 02115 doblen@neco.edu.

Declaration of interest: N. Doble was a founder of Iris AO Inc, the DM manufacturer. The other authors report no conflict of interest.

Author Manuscript Author Manuscript Author Manuscript Author Manuscript

myopia, respectively, again, within days.[3,4] Other uses for the chick eye include studies of the role of accommodation in eye growth control [3,5–8] and some retinopathies.[9–13]

Because all of these various conditions are associated with retinal signal processing or cellular pathologies (in the case of retinopathies), it would be advantageous to be able to image potential changes in the retina that might be occurring at the level of the photoreceptors. Histological techniques on excised tissue are of limited appeal due to the introduction of histological artifacts such as shrinkage, as well as the preclusion of longitudinal studies which yield valuable information on etiologies.

The Photoreceptors and the Optics of the Chick Eye

Like the human eye, the chick eye suffers from optical aberrations in the lens and cornea which limit the ability to visualize microscopic structure *in vivo*. Coletta et al.[14] examined the double pass point spread function (PSF) in 21 White Leghorn chickens (3 to 6 weeks of age, 2 to 5.25 mm pupil diameters). They concluded that the optical quality of the chick eye is worse than in human eyes but like the human eye the spatial resolution is not limited by the ocular optics. Thibos et al.[15] report that the higher order aberration magnitudes in the chick eye are larger than those observed in human eyes. However, other authors report better optical quality. Kisilak et al.[16] report a higher order aberration magnitude of 0.090 μm at day 0 decreasing to 0.042 μm at day 14 (1.6 mm pupil diameter). Similarly, Cera et al.[17] give a higher order aberration magnitude of 0.12 μm at day 0 decreasing to 0.03 μm at day 13.

These uncorrected aberrations will blur the images of the photoreceptors. We estimate the lateral resolution of a 6 week old chick eye to be approximately 2.5 μm (assumes a 2 mm pupil diameter, 7.5 mm focal length, and a wavelength of 550 nm), this should be sufficient to view single photoreceptors. From Bowmaker et al.[18] the single cone diameter was estimated to be 3.3 μm (2 week old birds). Lopez-Lopez et al.[19] estimate a 3.5 μm single cone diameter for 8 week old White Leghorn chicks, while Hart et al.[20] quote single cone oil droplet diameter values ranging from 3.2 to 4.0 μm for juvenile (10–18 weeks) and 3.2 to 4.7 μm for adults birds (25–33 weeks).

Obtaining the best *in vivo* retinal image quality requires correcting both the spatial and dynamic aberration changes, which can be achieved by applying adaptive optics (AO). AO is used extensively in the study of human retinal structure[21–25] and visual perception.[26–28] Kisilak et al.[29] and Zhang et al.[30] have published recent abstracts on the observation of chick photoreceptors *in vivo*, the latter employing AO in a confocal scanning laser ophthalmoscope.

The purpose of our experiments was to use AO in the imaging of the cone photoreceptor mosaic of the chick retina, and to compare the results to those from histological sections. It is hoped that AO will prove to be a useful technique in understanding the changes that may be occurring in various ocular pathologies at the level of the photoreceptors, very early in the etiology of a disease.

Author Manuscript Author Manuscript Author Manuscript Author Manuscript

Materials and Method

Subjects

2 six week old White Leghorn (*Gallus gallus domesticus*) chicks (chick A and chick B) were hatched in an incubator and raised in a temperature-controlled brooder from 1 day of age. The chicks were kept under a normal 12 hour light/12 hour dark cycle (7.30 AM for light onset and 7.30PM for light off). The average light intensity was kept at 300 lux during the light cycle. Food and water were supplied ad libitum. The right eye was used for all imaging.

All experiments were carried out in accordance with the National Institutes of Health Guide for Care and Use of Laboratory Animals, and with the authorization of the NECO Institutional Animal Care and Use Committee (IACUC).

In addition to the AO imaging the following procedures were employed to characterize the individual chick eyes:

Fundus Imaging—The field of view (FOV) of the AO system is small, approximately 2.5° and hence it is a challenge to determine the exact retinal location that is being imaged. A fundus camera (Topcon TRC-NW5 with Polaroid 600 film) was, therefore, used to acquire 45° images of the chick retina through a dilated pupil in green light. The choroidal vasculature and pecten from these fundus photographs were then used as landmarks to determine the specific retinal location of the AO images.

Axial Length Measurement—The axial length for each chick was obtained using high frequency A-scan ultrasonography (Panametrics Model 176599, sampling at 100MHz), using the procedure described by Nickla et al.[31] The axial length measurements were used in determining the magnification of the individual chick eye and hence the AO image scale in μm/pixel. This conversion is discussed further in the Materials and Methods section.

Refraction—Under isoflurane inhalation anesthesia, the chick's refractive error in both the 180° and 90° meridians was measured using a Hartinger's refractometer. The average of these values defined their spherical refraction. Table 1 summarizes the weight and the ocular biometric properties of chicks A and B.

AO Imaging

Optical Layout—The NECO AO fundus camera has not been described previously and hence is detailed here; its operation is similar to systems described by other authors.[21,23,32–35] The optical layout is shown in Figure 1 with the primary operating parameters detailed in Table 2. Briefly, the AO system employs a series of telescopes to relay the pupil plane (PP) of the chick eye to the microelectromechanical systems (MEMS) deformable mirror (DM)[36] and the wavefront sensor (WFS), which both lie in conjugate pupil planes. The same optics relay the retinal plane (RP) of the chick eye to the retinal conjugate plane at the imaging camera. A superluminescent diode (SLD) at 820±20 nm is used to measure the ocular aberration. The WFS samples the wavefront at 20 Hz and calculates the aberration coefficients up to 5th order in the OSA Zernike expansion.[37]

Author Manuscript Author Manuscript Author Manuscript Author Manuscript

Once good correction has been achieved (typically ~0.07 μm RMS over the 2 mm chick pupil) the shutter is opened to allow a 10 msec retinal exposure from the arc lamp. The visible light is reflected of the dichroic beamsplitter (BS1) and focused onto the imaging camera.

The AO system was primarily developed for human imaging over a 6 mm diameter pupil and hence extra optics (labeled 'chick imaging subsystem') were added to provide a 3-fold pupil demagnification. Light was redirected vertically downwards to allow for the chicks to be mounted in the prone position. A plane mirror was placed in the PP normally used for human subjects to allow for manual scanning of the chick retina. This arrangement allowed for a 12° range both horizontally and vertically and was calibrated so that each mirror adjustment could be tracked to 1° of movement in any direction.

Chick Preparation—Cycloplegic (Norcuron, Organon Inc) was administered to the right eye of the chick at an interval of 1 drop every 5 minutes for a total of 5 drops. When the last drop of the cycloplegic was administered the chick was then anesthetized with combination of Ketamine HCl (Phoenix Pharmaceuticals Inc, 100 mg/mL) and Xylazine (Phoenix Pharmaceuticals Inc, 20 mg/mL). The injected volume was determined by the ratio of the chick weight in grams (gm) to the volume of the drug in microliters (μL). The relationship was 1:1 for Ketamine and 4:1 for Xylazine. For example, a 100 gm chick would receive 100 μL Ketamine and 25 μL Xylazine. Imaging was performed 10 minutes after the Ketamine/ Xylazine injection.

Chick Alignment—The chick was mounted in the prone position on a 5-axis optical stage (XYZ and tip/tilt) to provide accurate co-alignment of the pupil with the WFS and DM. The head was secured via a Velcro strap to the stage with the chick's right eye facing upwards. A lid retractor was used, with the eye being kept hydrated through regular application of Refresh Plus lubricant eye drops (Allergan). The chick was then adjusted vertically so that its pupil was one focal length from the last lens in the AO system. A temporary mirror was inserted in the chick imaging subsystem allowing for visualization of the retina with a hand held, direct ophthalmoscope. The chick was aligned using the 5-axis stage to view a feature of interest (e.g. the pecten). Fine adjustment was achieved using the manual scanning mirror.

Imaging Procedure—Each AO image spanned a 2.5° field of view, with an average of 12 images being taken at one location. Images were chosen based on a subjective measure of the cone image quality by the system operator. After sufficient images were collected, the manual scanning mirror was then adjusted to move to the next retinal location. The pecten was used as a landmark throughout the experiments. The limitations of the chick mounting hardware and the system optics restricted the range of retinal locations that could be imaged. The most central location that could be imaged was the nasal, ventral field: 36° nasal-12° superior retina for chick A and 40° nasal-12° superior retina for chick B (measured from the pecten tip). For chick B, an area of ±10° around the pecten was imaged in detail to investigate the variation in cone density and packing across this area.

Author Manuscript Author Manuscript Author Manuscript Author Manuscript

Image Processing

Registration and Montaging of AO images: Custom software written in Matlab (Mathworks, Natick, MA) was used to register and analyze the images.[38] The 12 images from one location were registered together to improve the signal to noise ratio. The registered images were then put through a mean filter with a 2 pixel radius (ImageJ, U. S. National Institutes of Health, Bethesda, Maryland) to average out the image noise. The process was then repeated at adjacent locations and the registered images were finally montaged together.

Scaling of AO images: The montaged images were scaled using the ultrasound measurements in Table 1. Individual scaling coefficients and lateral resolution were derived using a detailed layout modeled in ZEMAX optical design software (ZEMAX Development Corporation, Bellevue, WA). Parameters including the chick optics, AO system and any additional trial lenses (both sphere and cylinder lens corrections) along with the axial position of the imaging camera were incorporated into the model. Chick corneal and lens curvatures were determined based on the work of Schaeffel and Howland[39] and a homogenous lens refractive index model was used for modeling. The corneal curvatures were adjusted slightly to account for the second order refractions measured with the refractometer. The scaling coefficients in μm per pixel were then applied to the montaged images. The calculated lateral resolutions for chicks A and B were 2.56 μm and 2.61 μm respectively (pupil diameter of 2 mm, an imaging wavelength of 550 nm and the axial lengths given in Table 1; sufficient to resolve the cones and double cones.[19,20,40] Experimentally, the AO system magnification had previously been verified with the ZEMAX predictions using a calibrated model eye.

Cone density measurement: The montage and scaled images were then analyzed by an automated Matlab cone counting program[38]. The Xue et al [38] algorithm selects cones as a function of peak intensity and nearest neighbor distance (NND), both parameters can be adjusted by the operator. If the peak intensity is chosen to be too high, then dimmer cones may not be counted, whereas if it is too low, the noise in the image will be included. The initial user defined estimate of NND specifies the minimum distance that must exist between two cones for them to be counted as individual cells and is generally set to be approximately the FWHM of the Gaussian intensity profile of an individual cone. A correct estimate for the NND parameter will avoid the situation where bright pixels belonging to a single cone are counted as multiple cones. Hence, the program will only select adjacent cones that are at least one NND distance from the particular cone under study. The algorithm then looks at an individual cone and determines the distance to its nearest neighbor. This is repeated for every cone in the image. The NND is then reported as the range of these values throughout the image. Both parameters were empirically determined through comparison with manual cone counting over the same retinal area by two naive human observers. One location was selected from the ventral area of both birds, the difference between the values of the cone density from the automated and manual counting methods was ±2.5%. An absolute error in the cone numbers would require a comparison to histological counts from the same retinal area, this was not performed.

Author Manuscript Author Manuscript Author Manuscript Author Manuscript

Cone packing characteristics: A Voronoi analysis program written in Matlab was used to determine the size of the retinal area surrounding a particular cone that is closer to it than to any other cones. The mosaic regularity can then be determined by counting the number of vertices of these areas. As an example, for a perfect hexagonally packed photoreceptor mosaic one would expect 6 vertices (i.e. nearest neighbors) for each cone. Voronoi analysis has been used by several authors to investigate cell packing in primate and animal retina.[41–44]

RESULTS

AO Performance: Correction of the Chick Ocular Aberration

For the 2 mm pupil, the starting root mean square error (RMS) before AO correction was 0.23±0.01 μm, the peak to valley error (P-V) was 1.37±0.03 μm. After closing the AO loop, the RMS and the P-V were reduced to 0.07±0.01 and 0.40±0.08 μm respectively. For chick A, similar before and after AO measurement values were recorded albeit with a trial lens correction to remove the higher second order aberration.

High Resolution AO Imaging

Figure 2A and 2D shows the two montaged fundus photographs for both chicks and the location of the AO imaging (indicated by white rectangles). The underlying choroidal blood vessels are clearly visible. The fundus photographs were rotated so that the axis of the pecten was vertical with the origin of the coordinate system which is taken to be the tip of the pecten shadow. A series of calibrated concentric rings were then overlaid on this coordinate system with a retinal location specified by a set of Cartesian coordinates in degrees. The montaged AO images for both chick A and B (Figure 2C and 2F) for each retinal location could then be determined precisely by finding the identical vasculature on the fundus photographs – Figure 2B and 2E respectively.

Figure 3 is an example of the image analysis procedure for the 1° FOV AO images acquired at the various positions throughout the montage. Figure 3A shows a subsection of the montage which was analyzed to determine the cones centers. Figure 3B shows the position of the cone centers from which the cone density and NND could be determined. The cone centers were then used in the Voronoi analysis to determine the number of vertices (or nearest neighbors) and the area of each Voronoi domain – (Figure 3C).

From Figure 2C the calculated cone density measurement for chick A was 21,714±543 cones/mm^2 with a NND range of 4.1 to 8.0 μm. The spatial mosaic pattern was primarily hexagonal at 43%, with each cone having nearest neighbors with a localized Voronoi cone domain size of 51.1±15.6 μm^2. For chick B, analysis of Figure 2F gave a cone density of 26,105±653 cones/mm^2 with NND range of 4.3 to 7.9 μm. Voronoi analysis gave 43% 6 sided vertices with each cone having a domain of 45.5±10.7 μm^2. This cone density for chick B at this retinal location was higher than from chick A with a correspondingly shorter NND.

Author Manuscript Author Manuscript Author Manuscript Author Manuscript

Cone Density Surrounding the Pecten

The imaging procedure was extended for chick B to examine the cone mosaic immediately surrounding the pecten. The retina was imaged out to an eccentricity of ±10° in both the nasal and temporal superior fields. Figure 4 shows the fundus photograph with the AO images overlaid. The inset figure shows the location of the 11 measurement areas. Locations were chosen so that the cone density could be determined in both the radial and tangential directions.

Eleven retinal locations were examined and the results are presented in Table 3. For each retinal location, a 1° retinal patch was analyzed.

The density of cone photoreceptors surrounding the pecten varied from 20,980±524 to 25,148±629 cones/mm^2 with the nearest neighbor distance range of 4.3 to 8.2 μm. The related Voronoi analysis was primarily 6 vertices at 42% with 4 and 7 vertices prevalence at 29% and 20% respectively for each cone with a domain varying from 40.8±9.8 to 48.8±10.7 μm^2. As only one bird was examined we cannot determine whether there is a statistically significant variation in cone density with retinal location.

DISCUSSION

A comparison of the cone densities measured from the in-vivo AO images to previous histological studies is shown in Table 4.

Our mean cone density of approximately 23,000 cones/mm^2 was much higher than that found by Morris et al.[45] (16,576 cones/mm^2 in central retina and 13,760 cones/mm^2 in the periphery) and Bowmaker et al.[18] (about 10,000 cones/mm^2 in central retina). We do, however, show good agreement with Meyer and May who report a cone density of 21,850 cones/mm^2 in adult chickens. Both Morris et al.[46] and Meyer et al.[40] report that the chick retina has a uniform photoreceptor density, except for an afoveate area centralis (aster) located about 2 mm from the dorsal end of the optic disc. It should be noted that it is difficult to precisely compare our locations with those other authors, and that the variation in age between studies may account for some of the differences.

A more recent study by Kram et al.[41] examined the chick photoreceptor packing as a function of the individual cone type but did not look at the ensemble cone density. The availability of their cone data (a supplemental spreadsheet to their paper) did allow for the reconstruction of their ensemble cone mosaics. The results from their study could then be directly compared to the work presented here. The Matlab analysis programs[38] found that the Kram densities were higher than our measurements with values in the dorsal nasal field in the region of 28,307 to 35,961 cones/mm^2. Table 3 summarizes the cone densities, NND and the Voronoi area as a function of vertex number for the Kram data.

Figure 5A shows the variation in the number of Voronoi vertices[41] for each of the 11 locations imaged around the pecten for chick B, also shown are the equivalent plots for the 6 Kram locations. As can be seen both datasets show the same trend, with the majority of cones having 6 nearest neighbors, i.e. a preference towards hexagonal packing.

Author Manuscript Author Manuscript Author Manuscript Author Manuscript

Kram et al. [41] also introduced another measure of the topological disorder (μ_2) which is the variance of the probability distribution P_n of the number of sides, n for a particular cone, $\mu_2 = (2\pi P_6^2)^{-1}$. Figure 5B shows the topological disorder as function of the fraction of hexagons. The 11 locations from the AO imaging and the 6 retinal locations from Krams data (Table 3) fall on the curve predicted by Lemaitre's law in the range $0.34<P6<0.66$.

The variation between our results and that of Kram et al.[41] in terms of NND and Voronoi domain area is due in part to the difference in the age of the chicks. From the Kram et al.[41] data using 15 day old chicks, the NND for the ensemble of cones was determined to be 2.9±0.8 μm in the ventral field- (Table 4). If we extrapolate this cone separation for a six week old chick using the values of Schaeffel and Howland,[39] our ZEMAX modeling predicts a NND of 3.8±0.8 μm, which is closer to our measured values of 5.1±0.7 and 5.3±0.8μm in the ventral field.

The present *in vivo* study is not able to differentiate between the double cones and the various types of single cones although this has been performed by other authors *in vitro*[41]. Due to our lateral resolution of 2.5–2.6 μm, we are not able to resolve the auxiliary cone of the double cones, which we estimate from Bowmaker et al.[18] to be approximately 1.1 μm in diameter and also the much smaller rods.[45] Our density calculations assume that we are imaging the single and double cones and that each appears as a single, bright object in our retinal images. It may be possible, in the future, to differentiate between the single cone types by employing retinal densitometry measures similar to those detailed by Roorda and Williams[47] for the human eye. However, the *in vivo* imaging situation is further complicated in the chick retina due to the larger number of cone pigments and their relative proximity in terms of spectral sensitivity.[48]

In summary, previous retinal studies examining photoreceptor density measurements in chicks have relied on *in vitro* histological analysis. Our results show that AO imaging enables single cone photoreceptor resolution and is an effective method of measuring cone parameters in the living chick eye.

Acknowledgments

This study was supported by a National Eye Institute T35 summer research training grant (NIH-EY007149). The authors thank Kenneth Chung, Heather Melanson, and Joyce Wei for the imaging assistance as well as Rachel Currin, Oesa Eng, and Maria Walker for Matlab analysis of the images. We would like to thank Kristen Totonelly for assistance and training with ultrasound and refraction. Also, we are grateful to Dr. Francis Rucker (New England College of Optometry) for advice and direction with chick modeling and Dr. Joseph Corbo (Washington University, School of Medicine, St Louis) for useful discussion.

References

1. Wallman J, Winawer J. Homeostasis of eye growth and the question of myopia. Neuron. 2004; 43:447–468. [PubMed: 15312645]
2. Wallman J, Turkel J, Trachtman J. Extreme myopia produced by modest changes in early visual experience. Science. 1978; 201:1249–1251. [PubMed: 694514]
3. Schaeffel F, Troilo D, Wallman J, Howland HC. Developing eyes that lack accommodation grow to compensate for imposed defocus. Vis Neurosci. 1990; 4:177–183. [PubMed: 2271446]
4. Wildsoet C, Wallman J. Choroidal and scleral mechanisms of compensation for spectacle lenses in chicks. Vision Res. 1995; 35:1175–1194. [PubMed: 7610579]

Author Manuscript Author Manuscript Author Manuscript Author Manuscript

5. Schaeffel F, Howland HC, Farkas L. Natural accommodation in the growing chicken. Vision Res. 1986; 26:1977–1993. [PubMed: 3617538]
6. Schaeffel F, Howland HC. Corneal accommodation in chick and pigeon. J Comp Physiol. 1987; 160:375–384. [PubMed: 3572853]
7. Schaeffel F, Glasser A, Howland HC. Accommodation, refractive error, and eye growth in chickens. Vision Res. 1988; 28:639–657. [PubMed: 3195068]
8. Choh V, Sivak J. Lenticular accommodation in relation to ametropia: the chick model. J Vis. 2005; 5:165–176. [PubMed: 15929643]
9. Montiani-Ferreira F, Fischer A, Cernuda-Cernuda F, Kiupel M, DeGrip W, Sherry D, Cho S, Shaw G, Evans M, Hocking P, Petersen-Jones S. Detailed histopathologic characterization of the retinopathy, globe enlarged (*rge/rge*) chick phenotype. Molecular Vision. 2005; 11:11–27. [PubMed: 15660021]
10. Montiani-Ferreira F, Li T, Kiupel M, Howland H, Hocking P, Curtis R, Petersen-Jones S. Electroretinographic features of the retinopathy, globe enlarged (rge) chick phenotype. Vision Res. 2003; 43:2009–2018. [PubMed: 12842154]
11. Boote C, Hayes S, Young R, Kamma-Lorger C, Hocking P, Elsheikh A, Inglehearn C, Ali M, Meek K. Ultrastructural changes in the retinopathy, globe enlarged (rge) chick cornea. J Struct Biol. 2009; 166:195–204. [PubMed: 19258040]
12. Fischer A, Scott M, Tuten W. Mitogen-activated protein kinase-signalling stimulates Muller glia to proliferate in acutely damaged chicken retina. Glia. 2009; 57:166–181. [PubMed: 18709648]
13. Finnegan S, Robson J, Hockin P, Inglehearn C, Stitt A, Curry W. Proteonomic profiling of the retinal dysplasia and degeneration chick retina. Mol Vis. 2010; 11:7–17.
14. Coletta N, Marcos S, Wildsoet C, Troilo D. Double-pass measurement of retinal image quality in the chicken eye. Opt & Vis Sci. 2003; 801:50–57.
15. Thibos L, Cheng X, Phillips J, Collins A. Optical aberrations of chick eyes. Invest Ophthalmol Vis Sci. 2002; 43:180.
16. Kisilak ML, Campbell MCW, Hunter JJ, Irving EL, Huang L. Aberrations of chick eyes during normal growth and lens induction of myopia. J Comp Phys A. 2006; 192:845–855.
17. García de la Cera E, Rodríguez G, Marcos S. Longitudinal changes of optical aberrations in normal and form-deprived myopic chick eyes. Vision Res. 2006; 46:579–589. [PubMed: 16051309]
18. Bowmaker J, Knowles A. The visual pigments and oil droplets of the chicken retina. Vision Res. 1977; 17:755–764. [PubMed: 898682]
19. Lopez-Lopez R, Lopez-Gallardo M, Perez-Alvarez MJ, Prada C. Isolation of chick retina cones and study of their diversity based on oil droplet colour and nucleus position. Cell Tissue Res. 2008; 332:13–24. [PubMed: 18266011]
20. Hart NS, Lisney TJ, Collin SP. Cone photoreceptor oil droplet pigmentation is affected by ambient light intensity. J Exp Biol. 2006; 209:4776–4787. [PubMed: 17114410]
21. Liang J, Williams D, Miller D. Supernormal vision and high-resolution retinal imaging through adaptive optics. J Opt Soc Am A. 1997; 14:2884–2892.
22. Hofer H, Carroll J, Neitz J, Neitz M, Williams DR. Organization of the human trichromatic cone mosaic. J Neuroscience. 2005; 25:9669–9679. [PubMed: 16237171]
23. Choi SS, Doble N, Hardy JL, Jones SM, Keltner JL, Olivier SS, Werner JS. In-vivo imaging of the photoreceptor mosaic in retinal dystrophies and correlations with retinal function. Invest Ophthalmol Vis Sci. 2006; 47:2080–2092. [PubMed: 16639019]
24. Wolfing J, Chung M, Carroll J, Roorda A, Williams DR. High-resolution retinal imaging of cone–rod dystrophy. Ophthalmology. 2006; 113:1014–1019.
25. Roorda A, Zhang Y, Duncan JL. High-resolution in vivo imaging of the RPE mosaic in eyes with retinal disease. Invest Ophthalmol Vis Sci. 2007; 48:2297–2303. [PubMed: 17460294]
26. Yoon GY, Williams DR. Visual performance after correcting the monochromatic and chromatic aberrations of the eye. J Opt Soc Am A. 2002; 19:266–275.
27. Artal P, Chen L, Fernández EJ, Singer B, Manzanera S, Williams DR. Neural compensation for the eye's optical aberrations. J Vision. 2004; 4:281–287.

Author Manuscript Author Manuscript Author Manuscript Author Manuscript

28. Chen L, Kruger PB, Hofer H, Singer B, Williams DR. Accommodation with higher-order monochromatic aberrations corrected with adaptive optics. J Opt Soc Am A. 2006; 23:1–8.
29. Kisilak ML, Hunter JJ, Irving EL, Campbell MCW. In vivo imaging of photoreceptors in the alert chicken. Invest Ophthalmol Vis Sci. 2007; 48:1191. [PubMed: 17325163]
30. Zhang Y, Xu J, Garcia M, Roorda A, Wildsoet C. In vivo imaging the photoreceptors in the chicken eye with adaptive optics scanning laser ophthalmoscope. J Vision. 2009; 9:79a.
31. Nickla D, Wildsoet C, Wallman J. Visual influences on diurnal rhythms in ocular length and choroidal thickness in chick eyes. Exp Eye Res. 1998; 66:163–181. [PubMed: 9533843]
32. Bartsch D, Zhu L, Sun P, Fainman S, Freeman W. Retinal imaging with a low-cost micromachined membrane deformable mirror. J Biomedical Opt. 2002; 7:451–456.
33. Larichev V, Ivanov P, Iroshnikov N, Shmalhauzen V, Otten L. Adaptive system for eye-fundus imaging. Quantum Electronics. 2002; 32:902–908.
34. Glanc M, Gendron E, Lacombe F, Lafaille D, Le Gargasson J, Lena P. Towards wide-field imaging with adaptive optics. Optics Comm. 2004; 230:225–238.
35. Rha J, Jonnal R, Thorn K, Qu J, Zhang Y, Miller D. Adaptive optics flood-illumination camera for high speed retinal imaging. Opt Express. 2006; 14:4552–4569. [PubMed: 19516608]
36. Helmbrecht, M., He, M., Juneau, T., Hart, M., Doble, N. Optomechatronic Micro/Nano Devices and Components II; Yoshitada Katagiri. Proc Soc Photo Opt Instrum Eng. Vol. 6376. Boston, MA: 2006. Segmented MEMS deformable-mirror for wavefront correction; p. 63760D1-63760D9.
37. Thibos LN, Applegate RA, Schwiegerling JT, Webb R. SIA Standards Taskforce Members [includes Salmon, T] Standards for reporting the optical aberrations of eyes. J Ref Surg. 2003; 18:S652–S661.
38. Xue B, Choi S, Doble N, Werner J. Photoreceptor counting and image montaging of en-face retinal images from an adaptive optics fundus camera. J Opt Soc Am A. 2007; 24:1364–1372.
39. Schaeffel F, Howland H. Visual optics in normal and ametropic chickens. Clin Vision Sci. 1988; 3:83–98.
40. Meyer D, May H. The Topographical distribution of rods and cones in the adult chicken retina. Exp Eye Res. 1973; 17:347–355. [PubMed: 4765257]
41. Kram Y, Manty S, Corbo J. Avian cone photoreceptors tile the retina as five independent, self-organizing mosaics. Plos One. 2010; 5:1–13.
42. Galli-Resta, Novelli E, Kryger Z, Jacobs GH, Reese BE. Modeling the mosaic organization of rod and cone photoreceptors with a minimal-spacing rule. European J Neuroscience. 1999; 11:1461–1469.
43. Baraas RC, Carroll J, Gunther KL. Adaptive optics retinal imaging reveals S-cone dystrophy in tritan color-vision deficiency. J Opt Soc Am A. 2007; 24:1438–1447.
44. Morgan J, Dubra A, Wolfe R, Merigan W, Williams D. In vivo autofluorescence imaging of the human and macaque retinal pigment epithelial cell mosaic. Invest Ophthalmol Vis Sci. 2009; 50:1350–1359. [PubMed: 18952914]
45. Morris V. Symmetry in a receptor mosaic demonstrated in the chick from the frequencies, spacing, and arrangement of the types of retinal receptor. J Comp Neurology. 1970; 140:359–398.
46. Morris V. An afoveate area centralis in the chick retina. J Comp Neurology. 1982; 210:198–203.
47. Roorda A, Williams DR. The arrangement of the three cone classes in the living human eye. Nature. 1999; 397(6719):520–522. [PubMed: 10028967]
48. Hart NS, Lisney TJ, Collin SP. Cone photoreceptor oil droplet pigmentation is affected by ambient light intensity. J Exp Biol. 2006; 209:4776–4787. [PubMed: 17114410]

Author Manuscript
Author Manuscript
Author Manuscript
Author Manuscript

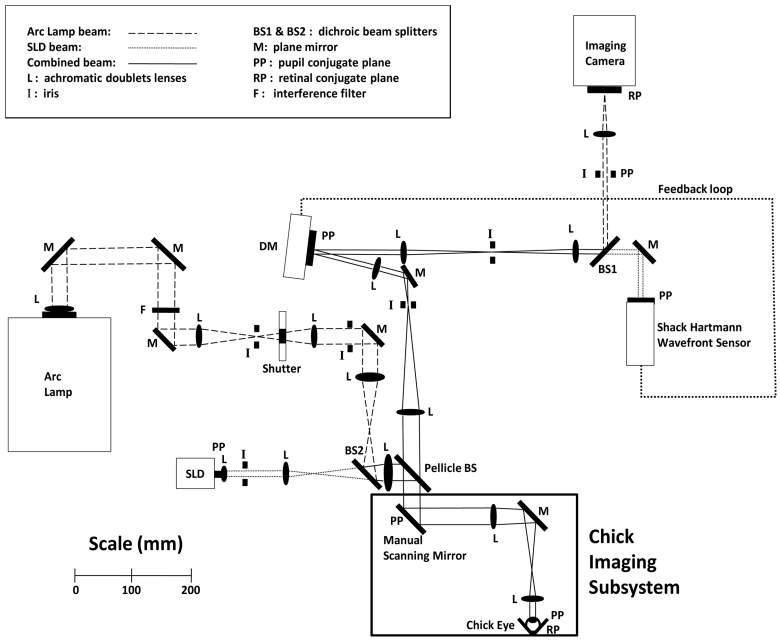

Figure 1.

Optical layout of the NECO AO fundus camera. The chick imaging subsystem redirects the normally horizontal optical path to be vertically downwards.

Author Manuscript Author Manuscript Author Manuscript Author Manuscript

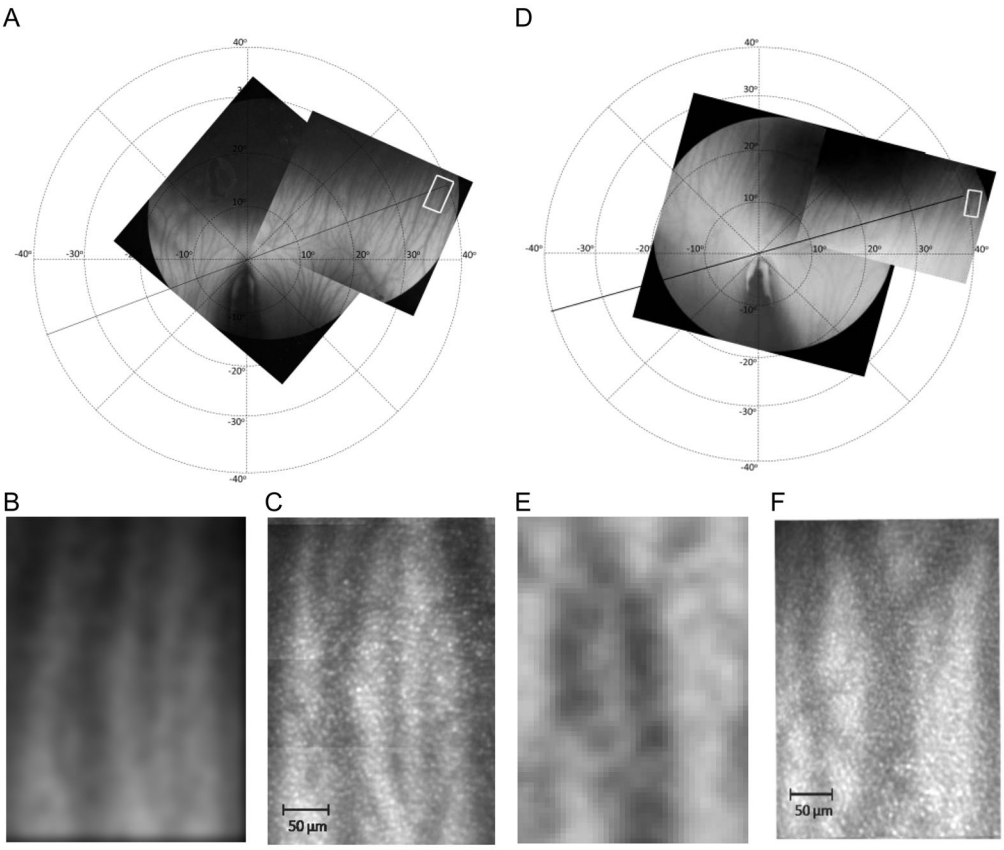

Figure 2.

(A) Montaged fundus photographs mapping the choroidal vasculature for chick A. The white rectangle indicates the retinal location where AO images were acquired i.e., 36° nasal and 12° superior from the tip of the pecten in the ventral field, (B) Cropped and enlarged fundus photograph from the white rectangle in (A) to show the landmark vasculature within the area, (C) Montaged AO image from the white box in (A): average cone density = 21,714±543 cones/mm^2, NND range of 4.1 to 8.0 µm, Voronoi analyses of 43% hexagonal, 28% pentagonal, 19% heptagonal and 10% other with a cone domain of 51.1±15.5µm^2 (D) Montaged fundus photographs mapping the choroidal vasculature for chick B. The AO images were acquired at 40° nasal and 12° superior from the tip of the pecten in the ventral field. (E) Cropped and enlarged fundus photograph from (D) (F) Montaged AO image from the white rectangle in (D): average cone density of 26,105±653 cones/mm^2 cones/mm^2, NND range of 4.3 to 7.9 µm, Voronoi analyses of 43% hexagonal, 28% pentagonal, 21% heptagonal and 8% other with a cone domain of 45.5±10.7 µm^2. All the AO images were taken with 550 nm imaging light.

Author Manuscript Author Manuscript Author Manuscript Author Manuscript

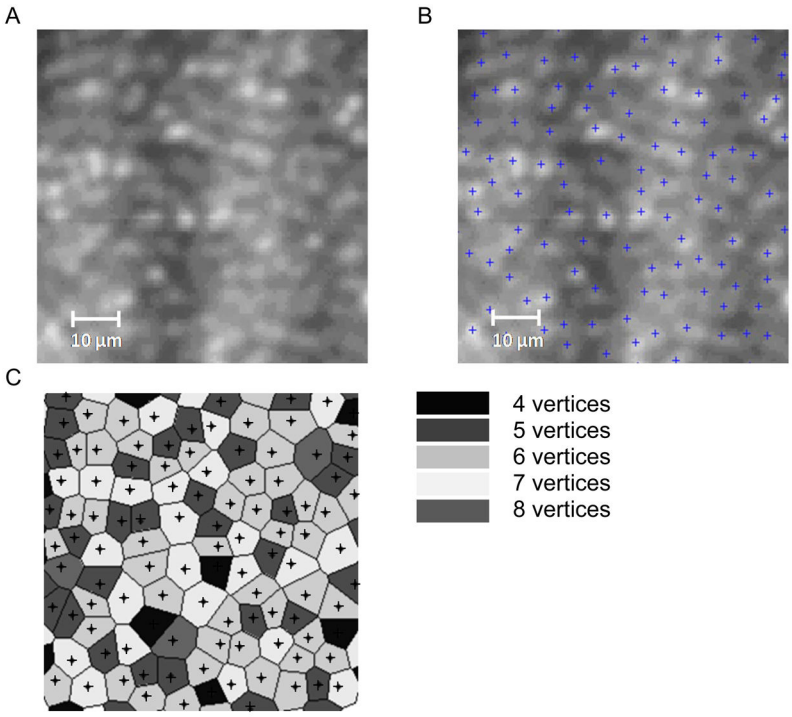

Figure 3.

Example of the cone analysis procedure. (A) a subsection of the registered and montaged retinal image (70 × 70 μm) centered at location (40°, 12°) for chick A, (B) shows the cone centers determined using the algorithms described by Xue et al. [38] (C) shows the cone centers surrounded by their individual Voronoi domains. The shading indicates the number of vertices.

Author Manuscript Author Manuscript Author Manuscript Author Manuscript

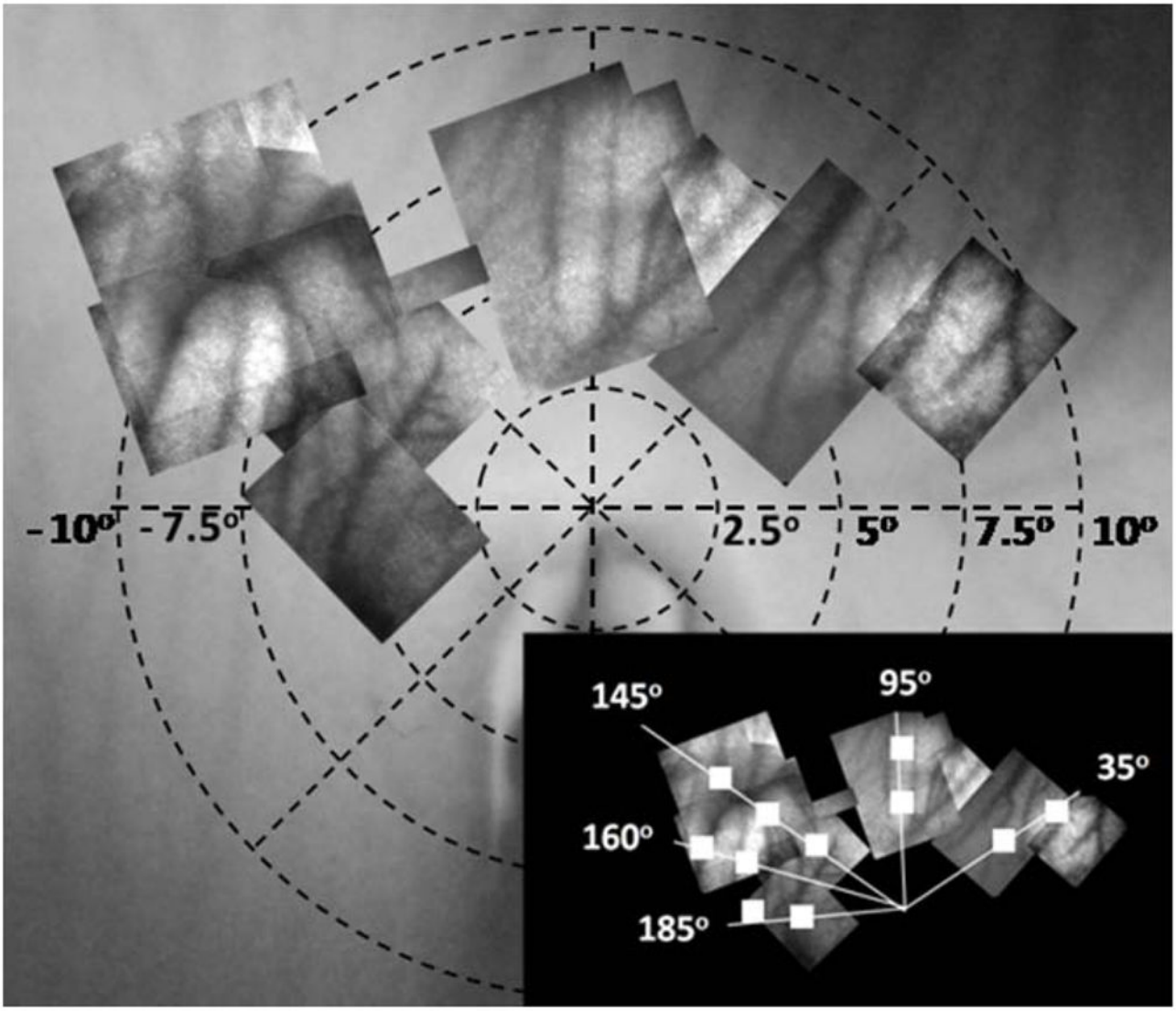

Figure 4.
Fundus image for chick B with overlapped montaged AO images spanning ±10° horizontally from the pecten. The 11 cone measurement locations are shown in the bottom right inset figure.

Author Manuscript Author Manuscript Author Manuscript Author Manuscript

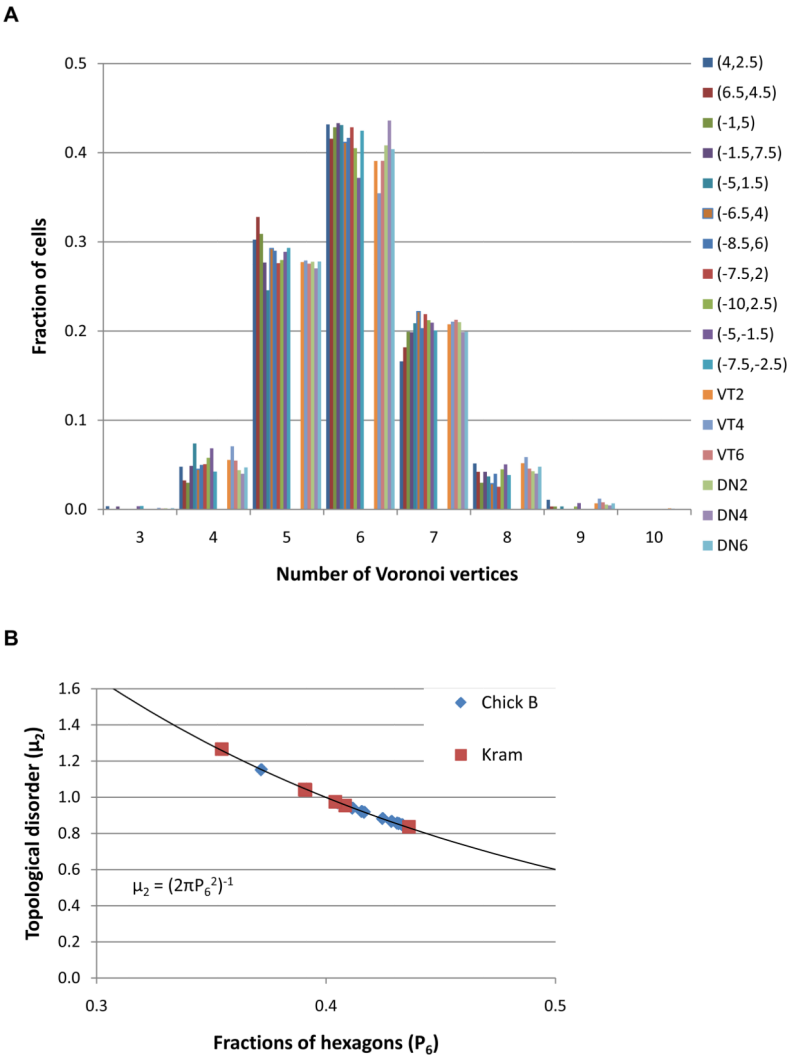

Figure 5.

(A) The fraction of cones cells as a function of Voronoi vertex number. The 11 retinal locations surrounding the pecten are shown for chick B. Also plotted are the 6 Kram et al[41] locations described in Table 3. Both datasets show a trend towards a hexagonal ordered photoreceptor array. (B) P_6 vs. topological disorder (μ_2) for the chick B locations compared to the Kram et al [41] locations. All data points fall on the curve predicted by Lemaitre's law in the range 0.34<P6<0.66.

Author Manuscript

Author Manuscript

Author Manuscript

Author Manuscript

Table 1

Weight and Optical Properties of the Two Chicks

	Chick A	Chick B
Age (weeks)	6	6
Weight (grams)	370	610
Refraction (diopters, D)	+3.8DS −.6DC × 180	+0.1DS
Anterior chamber depth (mm)	1.07	1.63
Lens thickness (mm)	2.99	3.05
Vitreous chamber depth (mm)	7.32	6.92
Sensory retina thickness (mm)	0.20	0.21
Axial Length (mm)	11.58	11.81
Focal length (mm)	7.64	7.79
Lateral resolution (μm)	2.56	2.61

Author Manuscript

Author Manuscript

Author Manuscript

Author Manuscript

Table 2

Operating Parameters for the NECO AO Fundus Camera

	PARAMETER	VALUE
	Pupil Diameter (chick eye)	2 mm
Wavefront Sensor	Type	Shack-Hartmann
	Pupil Diameter (WFS)	3.5 mm
	Lenslets	7×7 (hexagonal packing)
	Lenslet Pitch	0.6 mm
	Lenslet Focal Length	19 mm
	Zernike Reconstruction	Up to 5^{th} order
	WFS Source	SLD 820±20 nm
	Power (at chick cornea)	10 μW
	Beam Diameter	0.75 mm
	WFS Camera	Uniqvision UP-680-CL
	Sampling Frequency	20 Hz
Deformable Mirror	Manufacturer	Iris AO Inc
	Type	MEMS segmented piston/tip/tilt
	Segments	7 × 7 hexagonal packing
	Pitch (center to center)	606 μm
	Mirror Stroke	5 μm
	Inscribed Diameter	3.5 mm
	Refresh Rate	2.3 kHz
	Voltage	110 Volts
	Fill Factor	98.5 %
	WFS: DM Mapping	1:1
Imaging Channel	Source	Mercury Xenon 600W arc lamp
	Imaging Wavelength	550±40 nm
	Power (chick cornea)	50 μW
	Beam Diameter (chick cornea)	0.8 mm
	Exposure time	10 msec
	Imaging Camera	Photometrics Quantix KAF 1602E
	Field of View	2.5°

Author Manuscript Author Manuscript Author Manuscript Author Manuscript

Curr Eye Res. Author manuscript; available in PMC 2017 March 16.

Table 3

Eleven 1° FOV images were selected across the pecten field for chick B. Each location is designated by Cartesian coordinates (X,Y) with (0,0) being located at the tip of the pecten. For comparison the lower section of the Table 3 represents the 3 ventral/temporal (VT) locations and the 3 dorsal/nasal (DN) from Kram et al [41]. The difference in the Voronoi area is due in part to the difference in the age of the birds.

X (°)	Y (°)	Cone Density (Cones/mm^2)	NND Range (μm)	Voronoi Area per Vertex # (μm^2)		
				5	6	7
4	2.5	22,005 ± 550	4.3 – 8.2	42 ± 12	44 ± 10	49 ± 9
6.5	4.5	24,123 ± 603	4.3 –7.5	43 ± 13	42 ± 6	47 ± 7
−1	5	24,123 ± 603	4.3 –7.8	39 ± 8	42 ± 8	48 ± 7
−1.5	7.5	24,397 ± 609	4.3 –7.8	38 ± 9	42 ± 8	45 ± 8
−5	1.5	23,645 ± 591	4.3 –7.5	40 ± 10	46 ± 11	49 ± 11
−6.5	4	24,670 ± 617	4.3 –7.5	39 ± 11	41 ± 7	46 ± 8
−8.5	6	24,328 ± 608	4.3 –7.4	40 ± 10	43 ± 8	49 ± 8
−7.5	2	24,807 ± 620	4.3 –7.5	40 ± 12	42 ± 8	46 ± 11
−10	2.5	25,148 ± 629	4.3 –8.0	38 ± 10	40 ± 8	45 ± 8
−5	−1.5	22,483 ± 562	4.3 –7.8	41 ± 8	47 ± 11	52 ± 10
−7.5	−2.5	20,980 ± 524	4.3 –7.8	44 ± 11	48 ± 9	55 ± 9
Kram et al [41]						
VT2		21,986	2.7 – 4.8	25 ± 21	23 ± 16	25 ± 14
VT4		26,666	3.7 –6.3	25 ± 22	23 ± 17	24 ± 15
VT6		29,434	3.0 –3.7	18 ± 14	22 ± 18	20 ± 13
DN2		35,961	2.2 –3.3	12 ± 3	19 ± 16	20 ± 16
DN4		32,294	2.4 –5.4	19± 16	18 ± 16	19 ± 10
DN6		28,307	2.8 –3.6	19 ± 15	20 ± 15	21 ± 13

Author Manuscript

Author Manuscript

Author Manuscript

Author Manuscript

Table 4

Comparison of our study to previous histological studies reporting the photoreceptor density and spatial organization in the chick retina. (40°, 12°) represents the location 40° nasal and 12° superior to the pecten.

Retinal Location	Density Range (cones/mm^2)
Our Study (age: 6 weeks)	
Chick A (40°, 12°)	21,714±543
Chick B (40°, 12°)	26,105±653
Chick B at pectin	20,980 to 25,148
Kram et al. [41] *(age: 15 days)*	
DN	28,307 to 35,961
VT	21,986 to 29,434
Morris et al. [45] *(age: 2 weeks)*	
Center Retina	16,576
Peripheral Retina	13,760
Meyer and May [40] *(age: adult)*	
Not specified	21,850
Bowmaker et al. [18] *(age: 2 weeks)*	
Center Retina	10,021

DN = dorsal/nasal, VT = ventral/temporal